S1. PHASE CORRECTION:

For both the temperature-controlled experiments and the multi-center datasets, a phase correction for multi-echo complex acquisitions was performed. For bipolar and/or interleaved echo train acquisitions, phase correction is needed to produce complex-based PDFF maps. A phase correction method previously implemented by Hernando et al[1] was applied to all complex acquisition images. A linear phase offset was applied in the readout and phase-encoding directions before constructing PDFF maps by minimizing the difference in water and fat amplitudes between magnitude and complex fitting. This would subsequently minimize the PDFF map inaccuracies by reducing the phase irregularities across echoes.

As mentioned earlier however, magnitude-based fitting is more susceptible to temperature-related errors than complex-based fitting[2]. Because of this, and since we are minimizing the difference in water and fat amplitudes between magnitude and complex fitting, the effect of temperature on this phase correction method is unknown, potentially leading to residual phase errors. Also, in this work, we compare the effect of temperature on purely magnitude, purely complex, and hybrid fitting, as these three fitting methods are expected to have different sensitivity to temperature-related errors in the signal model. Because magnitude-based fitting was not applied after complex-based fitting as in Hernando et al[1], these phase errors may remain.

S2. TABLES:

| MR System | Site | Vendor | Model | Software Version | Field Strength (T) |
|---|---|---|---|---|---|
| 1 | 1 | General Electric | Signa HDxt | HD23.0_V02 | 1.5 |
| 2 | 1 | General Electric | Optima MR450w | DV26.0_R02/3 | 1.5 |
| 3 | 1 | General Electric | Signa Premier | RX27.0_R01/2 | 3 |
| 4 | 1 | General Electric | Signa PET/MR | MP26.0_R01 | 3 |
| 5 | 1 | General Electric | Signa Artist | DV26.0_R02/3 | 1.5 |
| 6 | 1 | General Electric | Discovery MR750 | DV26.0_R01/3 | 3 |
| 7 | 1 | General Electric | Signa Architect | DV26.0_R03 | 3 |
| 8 | 1 | General Electric | Signa HDxt | HD23.0_V02 | 1.5 |
| 9 | 2 | Philips | Ingenia | 5.3.1.1 | 3 |
| 10 | 2 | Philips | Ingenia | 5.4.1.0 | 3 |
| 11 | 2 | Philips | Ingenia | 5.4.1.0 | 1.5 |
| 12 | 3 | Siemens | Prisma | Syngo MR E11 | 3 |
| 13 | 3 | Siemens | Skyra | Syngo MR E11 | 3 |
| 14 | 4 | Siemens | Avanto | Syngo MR E11 | 1.5 |
| 15 | 4 | Siemens | Skyra | Syngo MR E11 | 3 |
| 16 | 5 | General Electric | Discovery MR750 | DV26.0_R01 | 3 |
| 17 | 5 | General Electric | Discovery MR750 | DV26.0_R01 | 3 |
| 18 | 6 | Siemens | Aera | Syngo MR E11 | 1.5 |
| 19 | 6 | Siemens | Skyra | Syngo MR E11 | 3 |
| 20 | 7 | Philips | Ingenia | 5.3.1.1 | 1.5 |
| 21 | 7 | Philips | Ingenia | 5.3.1.1 | 3 |
| 22 | 8 | Siemens | Aera | Syngo MR E11 | 1.5 |
| 23 | 8 | General Electric | Discovery MR750 | DV26.0_R01 | 3 |
| 24 | 8 | General Electric | Discovery MR750 | DV26.0_R01 | 3 |
| 25 | 9 | Philips | Ingenia | 5.3.0.3 | 1.5 |
| 26 | 9 | Philips | Ingenia | 5.3.0.3 | 3 |

**Table S1:** List of unique MR systems used in the multi-center study.

| MR System | Field Strength (T) | $TE_{init}$ (ms) | ΔTE (ms) | ETL | Readout | Number of Echo Trains | Flip Angle (°) | TR (ms) | Slice Thickness (mm) | FOV ($cm^2$) | Matrix |
|---|---|---|---|---|---|---|---|---|---|---|---|
| 1 | 1.5 | 1.66 | 2.30 | 6 | bipolar | 1 | 10 | 120 | 6 | 26x26 | 256x256 |
| 2 | 1.5 | 1.55 | 2.70 | 6 | bipolar | 1 | 10 | 120 | 6 | 26x26 | 256x256 |
| 2 | 1.5 | 1.55 | 2.61 | 6 | bipolar | 1 | 10 | 120 | 6 | 26x26 | 256x256 |
| 3 | 3 | 1.30 | 1.16 | 6 | bipolar | 2 | 10 | 120 | 6 | 26x26 | 256x256 |
| 4 | 3 | 1.14 | 0.83 | 8 | bipolar | 2 | 10 | 120 | 6 | 26x26 | 256x256 |
| 5 | 1.5 | 1.74 | 2.46 | 6 | bipolar | 1 | 10 | 120 | 6 | 26x26 | 256x256 |
| 5 | 1.5 | 1.76 | 2.48 | 6 | bipolar | 1 | 10 | 120 | 6 | 26x26 | 256x256 |
| 6 | 3 | 1.32 | 1.13 | 6 | bipolar | 2 | 10 | 120 | 6 | 26x26 | 256x256 |
| 7 | 3 | 1.34 | 1.21 | 6 | bipolar | 2 | 10 | 120 | 6 | 26x26 | 256x256 |
| 9 | 3 | 1.15 | 1.19 | 6 | monopolar | 1 | 10 | 121 | 10 | 50x50 | 384x384 |
| 9 | 3 | 1.15 | 1.15 | 6 | bipolar | 1 | 10 | 121 | 10 | 50x50 | 288x288 |
| 10 | 3 | 1.15 | 1.19 | 6 | monopolar | 1 | 10 | 121 | 10 | 50x50 | 384x384 |
| 10 | 3 | 1.15 | 1.15 | 6 | bipolar | 1 | 10 | 121 | 10 | 50x50 | 288x288 |
| 11 | 1.5 | 2.30 | 2.30 | 6 | monopolar | 1 | 10 | 121 | 10 | 42x42 | 288x288 |
| 11 | 1.5 | 2.30 | 2.30 | 6 | bipolar | 1 | 10 | 121 | 10 | 42x42 | 288x288 |
| 12 | 3 | 1.15 | 1.15 | 6 | bipolar | 1 | 10 | 150 | 10 | 42x42 | 160x160 |
| 12 | 3 | 1.15 | 1.15 | 6 | bipolar | 1 | 10 | 150 | 7 | 42x42 | 160x160 |
| 13 | 3 | 1.12 | 0.99 | 6 | bipolar | 1 | 10 | 150 | 10 | 42x42 | 128x128 |
| 13 | 3 | 1.15 | 1.15 | 6 | bipolar | 1 | 10 | 262 | 5 | 42x42 | 128x128 |
| 14 | 1.5 | 1.15 | 1.15 | 6 | bipolar | 1 | 10 | 160 | 10 | 42x42 | 160x160 |
| 14 | 1.5 | 1.12 | 0.99 | 6 | bipolar | 1 | 10 | 150 | 10 | 42x42 | 256x256 |
| 14 | 1.5 | 2.30 | 2.30 | 6 | bipolar | 1 | 10 | 150 | 10 | 42x42 | 256x256 |
| 14 | 1.5 | 2.30 | 2.30 | 6 | bipolar | 1 | 10 | 216 | 10 | 42x42 | 160x160 |
| 15 | 3 | 1.15 | 1.15 | 6 | bipolar | 1 | 10 | 199 | 10 | 42x42 | 160x160 |
| 15 | 3 | 1.12 | 0.99 | 6 | bipolar | 1 | 10 | 150 | 10 | 40x45 | 224x256 |
| 15 | 3 | 1.12 | 1.18 | 6 | bipolar | 1 | 10 | 150 | 10 | 40x45 | 224x256 |
| 15 | 3 | 1.15 | 0.96 | 6 | bipolar | 1 | 10 | 150 | 10 | 40x45 | 140x160 |
| 15 | 3 | 1.15 | 1.15 | 6 | bipolar | 1 | 10 | 150 | 10 | 40x45 | 224x256 |
| 16 | 3 | 1.32 | 1.13 | 6 | bipolar | 2 | 10 | 120 | 6 | 26x26 | 256x256 |
| 17 | 3 | 1.32 | 1.13 | 6 | bipolar | 2 | 10 | 120 | 6 | 26x26 | 256x256 |
| 18 | 1.5 | 2.30 | 2.30 | 6 | bipolar | 1 | 10 | 271 | 10 | 26x26 | 160x160 |
| 19 | 3 | 1.14 | 1.16 | 6 | bipolar | 1 | 10 | 150 | 5 | 26x26 | 160x160 |
| 20 | 1.5 | 2.30 | 2.30 | 6 | bipolar | 1 | 10 | 120 | 5 | 34x34 | 192x192 |
| 21 | 3 | 1.15 | 1.15 | 6 | bipolar | 1 | 10 | 120 | 5 | 34x34 | 192x192 |
| 22 | 1.5 | 2.30 | 2.30 | 6 | bipolar | 1 | 10 | 128 | 10 | 30x30 | 160x160 |
| 23 | 3 | 1.30 | 1.11 | 6 | bipolar | 2 | 10 | 120 | 6 | 26x26 | 256x256 |
| 24 | 3 | 0.93 | 1.21 | 6 | bipolar | 1 | 10 | 120 | 10 | 50x50 | 256x256 |
| 24 | 3 | 1.30 | 1.11 | 6 | bipolar | 2 | 10 | 120 | 6 | 26x26 | 256x256 |
| 25 | 1.5 | 2.30 | 2.30 | 6 | bipolar | 1 | 10 | 120 | 5 | 34x34 | 192x192 |
| 26 | 3 | 1.15 | 1.15 | 6 | bipolar | 1 | 10 | 120 | 5 | 34x34 | 192x192 |

**Table S2:** All unique magnitude-based CSE-MRI protocols used in the multi-center study. Some protocols were performed multiple times to produce the total 68 magnitude-based CSE-MRI acquisitions. For all acquisitions, vials were oriented along $B_0$ and a multi-echo spoiled gradient echo was used. Details of the MR systems are listed in Table S1. Abbreviations: ETL = echo train length, TE = echo time, TR = repetition time, FOV = field of view.

| MR System | Field Strength (T) | $TE_{init}$ (ms) | ΔTE (ms) | ETL | Readout | Number of Echo Trains | Flip Angle (°) | TR (ms) | Slice Thickness (mm) | FOV ($cm^2$) | Matrix |
|---|---|---|---|---|---|---|---|---|---|---|---|
| 2 | 1.5 | 0.91 | 1.46 | 6 | monopolar | 1 | 5 | 12.67 | 10 | 40x40 | 130x130 |
| 2 | 1.5 | 1.02 | 1.72 | 6 | monopolar | 1 | 5 | 14.11 | 10 | 40x40 | 104x104 |
| 2 | 1.5 | 1.12 | 1.94 | 6 | monopolar | 1 | 5 | 25.57 | 3 | 26x26 | 148x148 |
| 3 | 3 | 0.87 | 0.69 | 6 | monopolar | 2 | 3 | 5.84 | 10 | 44x44 | 144x144 |
| 3 | 3 | 1.09 | 0.88 | 6 | monopolar | 2 | 3 | 7.35 | 3 | 26x26 | 160x160 |
| 4 | 3 | 0.99 | 0.83 | 6 | monopolar | 2 | 3 | 7.32 | 8 | 40x40 | 104x104 |
| 4 | 3 | 1.08 | 0.94 | 6 | monopolar | 2 | 3 | 11.37 | 4 | 26x26 | 140x140 |
| 5 | 1.5 | 0.94 | 1.98 | 6 | monopolar | 1 | 5 | 14.08 | 8 | 40x40 | 130x130 |
| 5 | 1.5 | 0.94 | 1.98 | 6 | monopolar | 1 | 5 | 14.13 | 8 | 40x40 | 130x130 |
| 5 | 1.5 | 1.12 | 1.95 | 6 | monopolar | 1 | 3 | 23.71 | 3 | 26x26 | 148x148 |
| 6 | 3 | 0.88 | 0.70 | 6 | monopolar | 2 | 3 | 5.82 | 10 | 44x44 | 144x144 |
| 6 | 3 | 1.13 | 0.90 | 6 | monopolar | 2 | 3 | 7.38 | 3 | 26x26 | 150x150 |
| 7 | 3 | 0.94 | 0.78 | 6 | monopolar | 2 | 3 | 6.85 | 10 | 44x44 | 144x144 |
| 7 | 3 | 0.94 | 0.78 | 6 | monopolar | 2 | 3 | 6.71 | 10 | 44x44 | 144x144 |
| 7 | 3 | 1.09 | 0.94 | 6 | monopolar | 2 | 4 | 11.79 | 3 | 26x26 | 140x140 |
| 8 | 1.5 | 0.87 | 1.64 | 6 | monopolar | 1 | 5 | 11.79 | 10 | 40x40 | 256x256 |
| 8 | 1.5 | 1.11 | 1.79 | 6 | monopolar | 1 | 4 | 18.27 | 3 | 26x26 | 256x256 |
| 9 | 3 | 0.91 | 1.30 | 6 | monopolar | 1 | 3 | 10.00 | 5 | 34x34 | 256x256 |
| 9 | 3 | 0.97 | 0.71 | 6 | bipolar | 1 | 3 | 5.65 | 6 | 40x40 | 224x224 |
| 9 | 3 | 1.30 | 1.18 | 6 | bipolar | 1 | 3 | 10.00 | 5 | 40x40 | 224x224 |
| 11 | 1.5 | 0.92 | 0.66 | 6 | bipolar | 1 | 5 | 5.32 | 6 | 40x40 | 192x192 |
| 11 | 1.5 | 1.49 | 1.30 | 6 | bipolar | 1 | 5 | 10.00 | 5 | 22x22 | 160x160 |
| 12 | 3 | 1.21 | 1.25 | 6 | bipolar | 1 | 4 | 9.02 | 5 | 28x28 | 320x320 |
| 12 | 3 | 1.25 | 1.23 | 6 | bipolar | 1 | 3 | 10.00 | 5 | 28x28 | 160x160 |
| 16 | 3 | 0.88 | 0.70 | 6 | monopolar | 2 | 3 | 5.82 | 10 | 44x44 | 144x144 |
| 16 | 3 | 1.13 | 0.90 | 6 | monopolar | 2 | 3 | 7.38 | 3 | 26x26 | 150x150 |
| 17 | 3 | 0.88 | 0.70 | 6 | monopolar | 2 | 3 | 5.82 | 10 | 44x44 | 144x144 |
| 17 | 3 | 1.13 | 0.90 | 6 | monopolar | 2 | 3 | 7.38 | 3 | 26x26 | 150x150 |
| 19 | 3 | 1.25 | 1.24 | 6 | bipolar | 1 | 3 | 10.00 | 5 | 30x30 | 160x160 |
| 20 | 1.5 | 0.66 | 0.66 | 6 | bipolar | 1 | 5 | 5.32 | 6 | 40x40 | 192x192 |
| 20 | 1.5 | 0.98 | 0.98 | 6 | bipolar | 1 | 5 | 7.43 | 5 | 26x26 | 176x176 |
| 20 | 1.5 | 2.00 | 2.00 | 6 | bipolar | 1 | 3 | 13.30 | 5 | 34x34 | 224x224 |
| 20 | 1.5 | 2.00 | 2.00 | 6 | monopolar | 2 | 3 | 13.30 | 5 | 34x34 | 224x224 |
| 21 | 3 | 0.69 | 0.95 | 6 | monopolar | 2 | 3 | 5.55 | 10 | 40x40 | 192x192 |
| 21 | 3 | 0.71 | 0.97 | 6 | bipolar | 1 | 3 | 5.65 | 6 | 40x40 | 224x224 |
| 21 | 3 | 1.03 | 1.30 | 6 | monopolar | 2 | 3 | 10.00 | 5 | 34x34 | 224x224 |
| 21 | 3 | 1.18 | 1.30 | 6 | bipolar | 1 | 3 | 10.00 | 5 | 34x34 | 224x224 |
| 25 | 1.5 | 0.98 | 0.71 | 6 | bipolar | 1 | 5 | 5.69 | 6 | 34x34 | 176x176 |
| 25 | 1.5 | 2.00 | 2.00 | 6 | bipolar | 1 | 3 | 14.00 | 6 | 34x34 | 224x224 |
| 26 | 3 | 0.98 | 0.71 | 6 | bipolar | 1 | 3 | 5.69 | 6 | 34x34 | 192x192 |
| 26 | 3 | 1.30 | 1.19 | 6 | bipolar | 1 | 3 | 10.00 | 5 | 34x34 | 224x224 |

**Table S3:** All complex-based CSE-MRI protocols used in the multi-center study. Some protocols were performed multiple times to produce the total 60 complex-based CSE-MRI acquisitions. For all acquisitions, vials were oriented along $B_0$ and a multi-echo spoiled gradient echo was used. Details of the MR systems are listed in Table S1. Abbreviations: ETL = echo train length, TE = echo time, TR = repetition time, FOV = field of view.

S3. FIGURES:

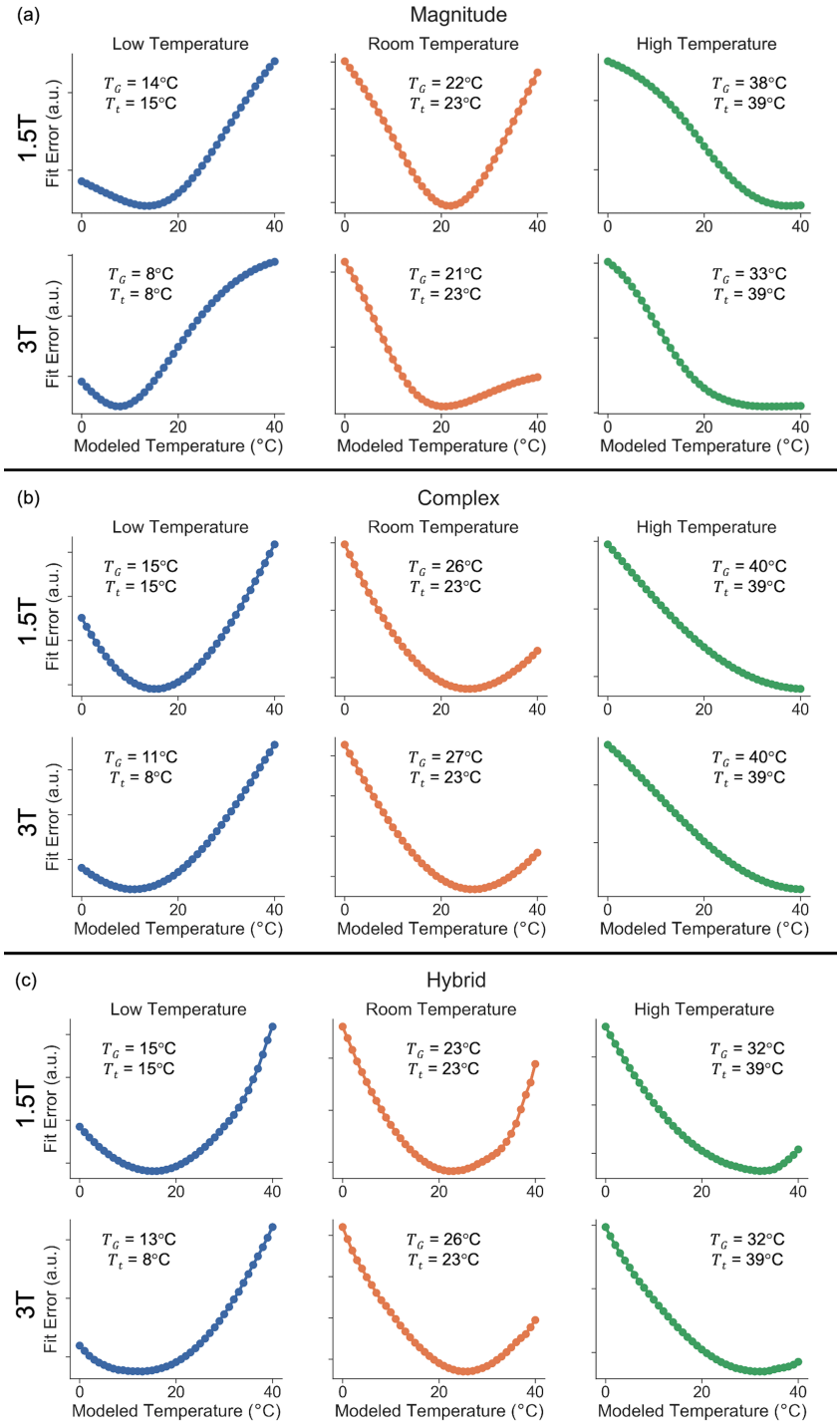


**Figure S1.** Global fit error can be used to estimate the true temperature of the phantom in order to correct for temperature-dependent errors in PDFF quantification. Fit error as a function of modeled temperature is shown in temperature-controlled experiments using two different field strengths (1.5T and 3T) at three different phantom temperatures (approximately 10°C, 20°C, 40°C) using a) magnitude-based b) complex-based c) hybrid-based methods. Global temperature at minimum fit error, $T_G$, and thermometer-measured phantom temperature, $T_t$ are shown.

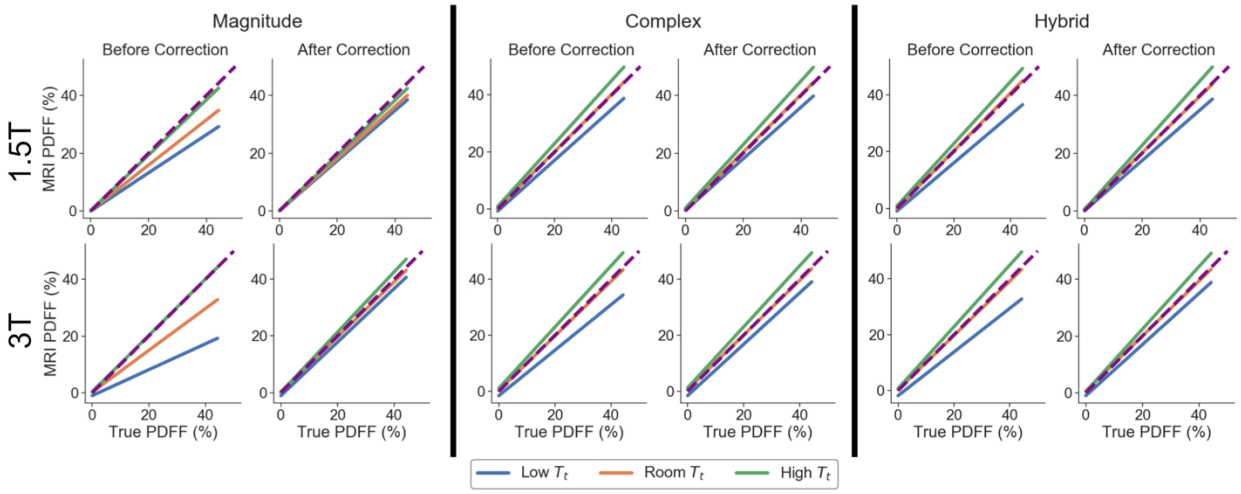


**Figure S2.** PDFF bias is reduced for all given true phantom temperatures ($T_t$) using the proposed temperature-correction method with $T_G$ found in Figure S1. Linear regression plots of MRI PDFF as a function of the true PDFF are shown for the temperature-controlled experiments at 1.5T and 3T, before and after temperature correction, using magnitude-based, complex-based, and hybrid-based methods. The identity line is also plotted as a dashed line.

S4. REFERENCES:


1. Hernando D, Sharma SD, Ghasabeh MA, et al. Multisite, multivendor validation of the accuracy and reproducibility of proton-density fat-fraction quantification at 1.5T and 3T using a fat–water phantom. *Magn Reson Med*. 2017;77(4):1516-1524. doi:10.1002/mrm.26228

2. Hernando D, Sharma SD, Kramer H, Reeder SB. On the confounding effect of temperature on chemical shift-encoded fat quantification. *Magn Reson Med*. 2014;72(2):464-470. doi:10.1002/mrm.24951